ChemComm

Accepted Manuscript

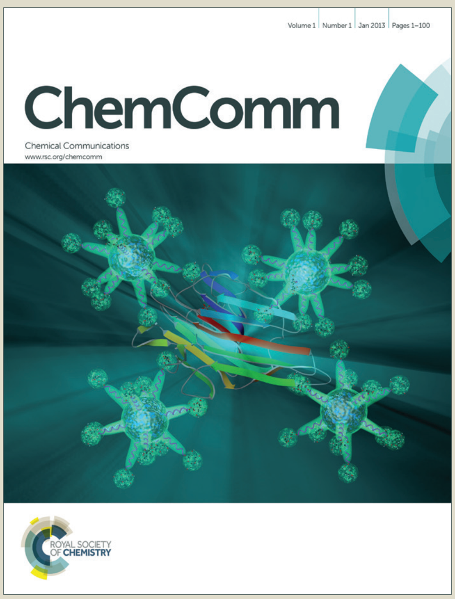

ChemComm

Journal Name

COMMUNICATION

Sulfurization of FeOOH Nanorods on a Carbon Cloth and their Conversion into Fe_2O_3/Fe_3O_4-S Core-Shell for Lithium Storage

Received 00th January 20xx,
Accepted 00th January 20xx

DOI: 10.1039/x0xx00000x

www.rsc.org/

Yang Luo,[a] Muhammad-Sadeeq Balogun,[a] Weitao Qiu,[a] Ruirui Zhao,[b] Peng Liu,[a] and Yexiang Tong*[a]

Fe_2O_3/Fe_3O_4-S CORE-SHELL NANORODS WERE FABRICATED ON A CARBON CLOTH BY SULFURIZATION OF FEOOH AND POST ANNEALING. THE PREPARED ELECTRODE EXHIBITED REMARKABLE CYCLIC STABILITY AND ATTRACTIVE RATE CAPABILITY FOR LITHIUM STORAGE.

Lithium-ion batteries (LIBs) have been invented and developed in the past decades.[1, 2] As a successful commercial product, LIBs have been widely used in portable electronic devices. Because LIBs possess the advantages of high energy density, long working life and environmental benignity and so on;[3, 4] they are considered as an important energy storage way to solve the energy crisis and much research attentions have been paid to them.[5, 6] To develop the next generation of LIBs for the demands of electric vehicles and large scale electrical energy storage grid, the anode materials of LIBs owing outstanding electrochemical performances play a key role.[7] Among the explored materials, iron-based materials (Fe_2O_3 and Fe_3O_4, mainly), which have many advantages, such as higher capacity (~1000 mA h g^{-1}), low cost, high safety and nontoxicity, will be the most promising candidate for the replacement of carbon anode (whose capacity is relatively low 372 mA h g^{-1}).[8, 9] However, low intrinsic electric conductivity and fast capacity fading still seriously hamper iron-based materials for practical using.[10]
In order to solve the above issues, a large number of methods have been proposed. Depending on the main characteristic of these methods, they can be divided into four kinds. First, design the nanostructure of the iron-based materials (particle size and morphology).[2, 11] Second, utilize the iron-based materials to construct hybrid with other materials.[12, 13] Third, dope other element in the iron-based materials.[13, 14] And lastly, coat carbon materials on the external of the iron-based materials.[15, 16] On the other hand, taking into consideration the individual properties of both Fe_2O_3 and Fe_3O_4, the combination of these oxides as LIB anode through a facile fabrication method are less reported.[17, 18] Thus, we proposed that the iron-based materials which consist of both Fe_2O_3 and Fe_3O_4 will possess high electrochemical performances and might be an effective way to overcome the problems hindering iron-based materials for practical using.

In this communication, we report a simple method to synthesize high performance Fe_2O_3-Fe_3O_4–S (FFS) core-shell nanorods on a carbon cloth as lithium ion batteries anode material. On account of the co-contribution of the Fe_2O_3 and Fe_3O_4 and the existence of conductive sulfur coated layer, the FFS presents high rate performance and long excellent cycling stability. The FFS core-shell nanorods exhibit 1213 mA h g^{-1}, 1090 mA h g^{-1}, 892 mA h g^{-1}, 728 mA h g^{-1}, 587 mA h g^{-1}, 414 mA h g^{-1} tested at 0.2 C, 0.5 C, 1 C, 3 C, 5 C and 10 C, respectively (1 C = 1000 mA h g^{-1}), and maintains 539 mA h g^{-1} after 100 cycles tested at 5 C.

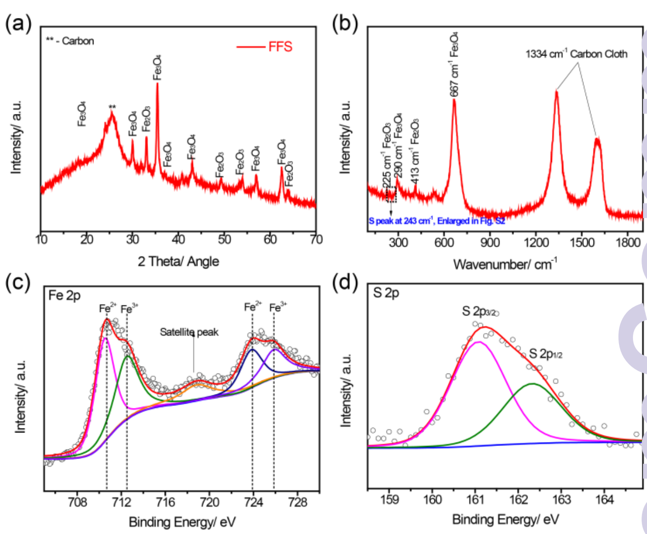

Fig. 1. Characterization of the FFS core-shell nanorods. (a) XRD profiles (b) Raman spectrum and (c, d) the high resolution XPS spectra of the S 2p and Fe 2p.

[a] MOE of the Key Laboratory of Bioinorganic and Synthetic Chemistry, KLGHEI of Environment and Energy Chemistry, The Key Lab of Low-carbon Chem & Energy Conservation of Guangdong Province, School of Chemistry and Chemical Engineering, Sun Yat-Sen University, 135 Xingang West Road, Chemical North Building 325, Guangzhou 510275, People's Republic of China; E-mail: chedhx@mail.sysu.edu.cn; Tel: +86-20-84110071; Fax: +86-20-84112245.
[b] EVE Industrial Park, Xikeng Industrial Zone, Huihuan Town, Huizhou, Guangdong, 516006, China.
† Footnotes relating to the title and/or authors should appear here.
Electronic Supplementary Information (ESI) available: [details of any supplementary information available should be included here]. See DOI: 10.1039/x0xx00000x

Firstly, FeOOH flower-like nanorods (Fig. S1) were fabricated on a carbon cloth by simple hydrothermal method according to our previous method (Experimental Section, Supporting Information, SI).[4] The carbon cloth was then immersed in 0.1 M thioacetamide for 6 h and then annealed in N_2 atmosphere at 400 ℃ for 60 mins to obtain the FFS core-shell nanorods. Thioacetamide was responsible for the partial reduction of Fe_2O_3 to Fe_3O_4 and sulfur coated layer upon annealing. Fig. 1a shows the XRD profile of the FFS nanorods. Intensed peaks of Fe_2O_3 and Fe_3O_4 were well observed, confirming the co-existence of the two oxides (PDF card no. #33-0664 and #19-0629, respectively). There were no traces of sulfur peaks due to the small amount in thioacetamide. Raman spectra collected for the FFS sample displayed Raman peaks of Fe_2O_3 at 225 and 413 cm^{-1} [19] and Fe_3O_4 at 290 and 667 cm^{-1}, [20] further affirming the co-existence of the two oxides (Fig. 1b). The enlarge Raman spectra of the FFS sample displayed in Fig. S2 shows the Raman peak of S at 243 cm^{-1} in the composite indicating the presence of S in the sample.

X-ray photoelectron spectroscopy (XPS) analyses were carried out to study the composition of the core-shell sample. Fig. 2c shows the high resolution XPS spectra of S 2p analyzed from the XPS survey (Fig. S3). The S 2p spectra of the FFS sample exhibit two peaks at 161.3 and 162.4 eV, which corresponds to S $2p_{3/2}$ and S $2p_{1/2}$, respectively of the S^{2-} oxidation state. [21, 22] This demonstrates that the presence S element in the nanorod. As shown in Fig. 1d, the Fe 2p XPS spectrum of the FFS exhibits two peaks at 710 and 724 eV, corresponding to Fe $2p_{3/2}$ and Fe $2p_{1/2}$ of the Iron oxides and a satellite peak of Fe_2O_3 at 718 eV. [23] Both Fe 2p peaks can further be deconvoluted into two broad peaks, namely Fe^{2+} and Fe^{3+}, which conform with the Fe 2p peaks of Fe_3O_4 and Fe_2O_3, [23, 24] further authenticating the co-existence of the iron oxides.

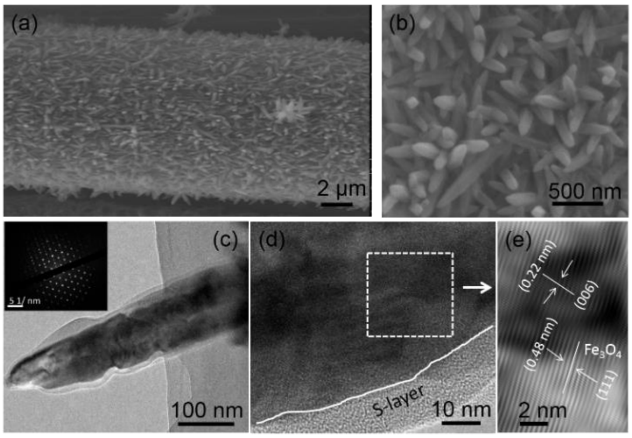

Fig. 2. Morphology of the FFS nanorod. (a and b) SEM images, (c) TEM image and (d) image displaying the lattice fringes spacing.

To gain an insight about the morphology of the FFS core-shell nanorods, Fig. 2 shows the scanning electron microscope (SEM), transmission electron microscope (TEM) and high-resolution TEM (HRTEM) images of the FFS core-shell nanorods. As shown in Fig. 2a and 2b, the FFS core-shell nanorods were homogeneously distributed on the carbon cloth, with diameters of 150-200 nm. Compared with the FeOOH nanorod, the FFS morphology exhibits a rough surface (Fig. 2b). Fig. 2c clearly reveals that the surface of the Fe_2O_3-Fe_3O_4 (core) is well coated by the S-layer (shell), and the thickness of the layer is about 10 nm (Fig. 2d). The energy dispersive X-ray spectroscopy (EDS) data revealed that the nanorods consist mainly of Fe, O and S elements, which are uniformly distributed in the nanorod (Figure S4). The enlarge HRTEM image in Fig. 2e shows that the fringe spacing of 0.22 nm agree well with the interplanar spacing (006) plane of the hematite Fe_2O_3 (PDF card no. #33-0664) and 0.48 nm, which corresponds with the (111) plane of the magnetite Fe_3O_4 (Fig. 2e) (PDF card no. #19-0629).

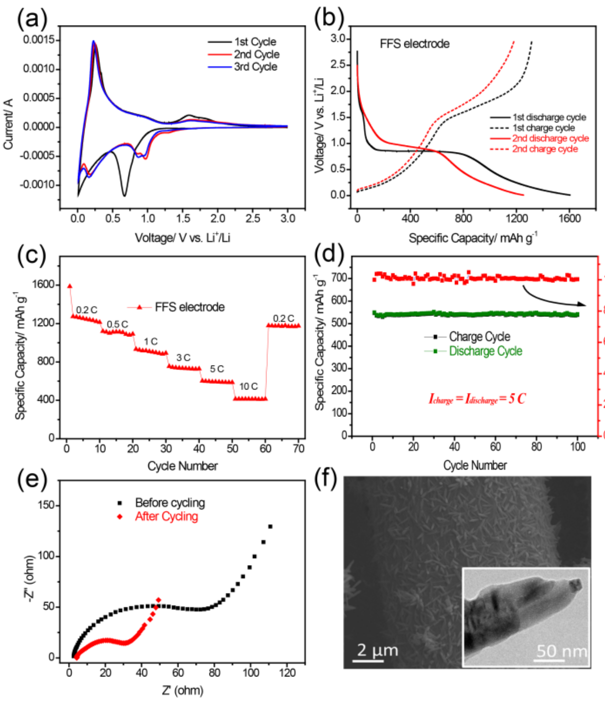

Fig. 3. (a) CV curve in the potential window of 0.01-3V at 0.01 mV s^{-1} scan rate, (b) Charge-discharge profiles at 0.2 C, (c) Rate performance at different current densities, (d) Cycling performance current density of 5 C for 100 cycles and (e) Nyquist plot of the FFS electrode. (f) SEM image of the electrode after cycling. Inset is the TEM image displaying the core-shell structure of the FFS electrode.

In order to test the electrochemical performance of the prepared FFS composite for application in lithium ion batteries, several electrochemical analysis were conducted. We used the optimized FFS-6h electrode for further electrochemical test (Fig. S5). Fig. 3a displayed the cyclic voltammetry (CV) of the FFS core-shell nanorod for the 1st, 2nd and 3rd cycles at a scan rate of 0.01 mV s between 0.01 V and 3 V. In the first cathodic process, the sample showed a large peak at 0.7 V, which indicated the transformation from Fe^{3+} and Fe^{2+} to Fe^0 and the formation of solid electrochemical interface (SEI) layer. [25, 26] An obvious peak appeared below 0.5 V, due to the reaction of lithium insertion and extraction in the carbon cloth. [3, 4, 27] Then there were two peaks at 1.63 V and 1.84 V, attributed to the oxidation of Fe^0 to Fe^{2+} and Fe^{3+}, respectively. [18] Compared with the first cycle, the subsequent cycles were quite different, and this was the result of the structural modification after the first cycle due to lithium insertion and extraction. [18] As can be seen from the charge-discharge profile, the first-cycle discharge capacity of the FFS composites reaches 1600 mA h g^{-1} at the current density at 0.2 C and the second-cycle discharge capacity maintains at 1280 mA h g^{-1} (Fig. 3b). Also, an obvious voltage plateau appears at about 0.8 V during the initial discharge process, then the plateau moves to about 1.0 V during the second discharge process, which correspond to the result obtained in the CV profiles. Considering the capacity contribution from the carbon cloth, the carbon cloth contributed about 9% of the total capacity as calculated in the Supporting Information. [28] This indicated that the carbon cloth have less capacity contribution to the capacity of the FFS electrode. Meanwhile, the FFS composite was cycled at various current densities for ten cycles ranging from 0.2 to 10 C, then back to the initial current density of 0.2 C. As shown in Fig. 3c, the reversible specific capacities of the FFS composite were 1213 mA h g^{-1}, 1090 mA h g^{-1}, 892 mA h g^{-1}, 728 mA h g^{-1}, and 587 mA h g^{-1}, respectively, even tested at a high current density of 10 C, the composite still delivered a high reversible capacity of 414 mA h g^{-1}. When the current density back to 0.2 C, the capacity of the FFS composite also kept at 1175 mA h g^{-1}, confirming that the FFS electrode exhibiting excellent rate capability and reversibility. This result is higher than some of the recently reported iron oxide-based anode [8, 10, 18] and comparable to some other ones. [11, 22]

Besides, we used a high constant current density (5 C) to evaluate the cycling performance of the FFS composite of the same cell after 70 cycles of rate performance test. Fig. 3d showed a highly stable cycling performance profile of the FFS composite. After 100 charge-discharge cycles, a reversible capacity of 538 mA h g^{-1} can be retained, which is higher and comparable to some other iron-oxide based electrodes. [2, 9, 11, 18, 22] It demonstrated that the FFS composite material can bear high current density, meanwhile it could also deliver high reversible capacity with coulombic efficiency maintained at 100 %. Fig. 3e was the Nyquist plots of the FFS core-shell nanorod before and after cycling at a frequency range between 100 kHz and 0.1 Hz with a perturbation amplitude of 5 mV. It clearly suggested that the electrochemical impedance after cycling was much smaller than the impedance before cycling and because of the reduction of the electrochemical impedance, it made the charge transfer resistance smaller and lead to rapid electron transport during the electrochemical lithium insertion/extraction, which was the reason of the excellent cycling stability of the FFS core-shell nanorods. Such phenomenon is common for many iron-oxide based electrodes. [23] Fig. 3f was the SEM and TEM images of the FFS electrode after 100 cycles at a current density of 5 C. It showed that the nanorod structure of the samples did not have any obvious change but the coated shell disappears and the nanorod are slightly denser than those of the initial SEM image (Fig. 2a-b), further affirming the excellent structural stability of the FFS nanorods. The excellent performance of the FFS electrode can be attributed to the synergistic effect and co-contribution of the Fe_2O_3 and Fe_3O_4, the coating of the conductive sulfur layer, which could improve the conductivity of the electrode and the mechanical strength and capacity contribution from the carbon cloth substrate.

In summary, we successfully synthesized excellent electrochemical performance Fe_2O_3-Fe_3O_4–S (FFS) core-shell nanorods on a carbon cloth through a simple method and use as anode material for lithium ion batteries. XRD, Raman and XPS characterization results demonstrate that the FFS core-shell nanorods comprises of both Fe_2O_3 and Fe_3O_4, as well as S element. The FFS nanorod composite as anode deliver a high reversible capacity of 1600 mA h g^{-1} at 0.2 C. Meanwhile, the FFS electrode has a long-term cycling stability with about 95 % capacity retention, maintaining 538 mA h g^{-1} after 100 cycles at a high current density of 5 C. We believe that the high reversible capacity and long cycling stability of the Fe_2O_3-Fe_3O_4–S (FFS) nanorod composite attribute to the existence of both Fe_2O_3 and Fe_3O_4 with synergistic effect, S conductive coated layer as well as the carbon cloth support. Moreover, the FFS core-shell nanorods were synthesized on a carbon cloth, which could make the whole system a promising material to be utilized in the flexible lithium ion batteries.

Acknowledgements

We acknowledge the financial support of this work received by the Natural Science Foundation of China (21403306, 2127329_, and J1103305) and the Natural Science Foundations of Guangdong Province (S2013030013474).

References

1. J.-M. Tarascon and M. Armand, *Nature*, 2001, **414**, 359.
2. Z. Wang, D. Luan, S. Madhavi, C. Ming Li and X. Wen Lou, *Chem. Commun.*, 2011, **47**, 8061.
3. M.-S. Balogun, C. Li, Y. Zeng, M. Yu, Q. Wu, M. Wu, X. Lu and Y. Tong, *J. Power Sources*, 2014, **272**, 946.
4. M.-S. Balogun, M. Yu, Y. Huang, C. Li, P. Fang, Y. Liu, X. Lu and Y. Tong, *Nano Energy*, 2015, **11**, 348.
5. J. Qian, D. Qiao, X. Ai, Y. Cao and H. Yang, *Chem. Commun.*, 2012, **48**, 8931.
6. M.-S. Balogun, W. Qiu, W. Wang, P. Fang, X. Lu and Y. Tong, *J. Mater. Chem. A*, 2015, **3**, 1364.
7. D. Chao, X. Xia, J. Liu, Z. Fan, C. F. Ng, J. Lin, H. Zhang, Z. X. Shen and H. J. Fan, *Adv. Mater.*, 2014, **26**, 5794-5800.
8. X. Zhang, H. Liu, S. Petnikota, S. Ramakrishna and H. J. Fan, *J. Mater. Chem. A*, 2014, **2**, 10835.
9. J. Wang, L. Li, C. L. Wong, L. Sun, Z. Shen and S. Madhavi, *RSC Adv.*, 2013, **3**, 15316.
10. B. Jang, M. Park, O. B. Chae, S. Park, Y. Kim, S. M. Oh, Y. Piao and T. Hyeon, *J. Am. Chem. Soc.*, 2012, **134**, 15010.
11. F. Han, L. Ma, Q. Sun, C. Lei and A. Lu, *Nano Res.*, 2014, **7**, 1706.
12. M. Chen, W. Li, X. Shen and G. Diao, *ACS Appl. Mater. Interfaces*, 2014, **6**, 4514-4523.
13. W. Xie, S. Li, S. Wang, S. Xue, Z. Liu, X. Jiang and D. He, *ACS Appl. Mater. Interfaces*, 2014, **6**, 20334-20339.
14. C. F. Zheng, N. Meng and Q. Chen, *Nanoscale*, 2015, **7**, 3410.
15. N. K. Chaudhari, S. Chaudhari and J.-S. Yu, *ChemSusChem*, 2014, **7**, 3102.
16. W.-M. Zhang, X.-L. Wu, J.-S. Hu, Y.-G. Guo and L.-J. Wan, *Adv. Funct. Mater.*, 2008, **18**, 3941-3946.
17. J.-S. Xu and Y.-J. Zhu, *ACS Appl. Mater. Interfaces*, 2012, **4**, 4752-4757.
18. X. Dong, L. Li, C. Zhao, H.-K. Liu and Z. Guo, *J. Mater. Chem. A*, 2014, **2**, 9844.
19. Y. Zeng, Y. Han, Y. Zhao, Y. Zeng, M. Yu, Y. Liu, H. Tang, Y. Tong and X. Lu, *Adv. Energy Mater.*, 2015, **5**, 1402176.
20. C. Liang, T. Zhai, W. Wang, J. Chen, W. Zhao, X. Lu and Y. Tong, *J. Mater. Chem. A*, 2014, **2**, 7214.
21. W. Qiu, J. Xia, H. Zhong, S. He, S. Lai and L. Chen, *Electrochim. Acta*, 2014, **137**, 197.

22. W. Li, M. Li, S. Xie, T. Zhai, M. Yu, C. Liang, X. Ouyang, X. Lu, H. Li and Y. Tong, *CrystEngComm*, 2013, **15**, 4212.
23. J. Luo, J. Liu, Z. Zeng, C. F. Ng, L. Ma, H. Zhang, J. Lin, Z. Shen and H. J. Fan, *Nano Letters*, 2013, **13**, 6136.
24. X. Lu, Y. Zeng, M. Yu, T. Zhai, C. Liang, S. Xie, M. S. Balogun and Y. Tong, *Adv. Mater.*, 2014, **26**, 3148.
25. S. H. Lee, S.-H. Yu, J. E. Lee, A. Jin, D. J. Lee, N. Lee, H. Jo, K. Shin, T.-Y. Ahn, Y.-W. Kim, H. Choe, Y.-E. Sung and T. Hyeon, *Nano Lett.*, 2013, **13**, 4249.
26. B. Wang, J. S. Chen, H. B. Wu, Z. Wang and X. W. Lou, *J. Am. Chem. Soc.*, 2011, **133**, 17146-17148.
27. M.-S. Balogun, M. Yu, C. Li, T. Zhai, Y. Liu, X. Lu and Y. Tong, *J. Mater. Chem. A*, 2014, **2**, 10825-10829.
28. C. Guan, X. Wang, Q. Zhang, Z. Fan, H. Zhang and H. J. Fan, *Nano Lett.*, 2014, **14**, 4852-4858.